

NRC Publications Archive Archives des publications du CNRC

Nanoscale morphology and thermal properties of low insertion loss fiber Bragg gratings produced using the phase mask technique and a single femtosecond laser pulse

Hnatovsky, Cyril; Silva, Kasthuri De; Abdukerim, Nurmemet; Walker, Robert B.; Ding, Huimin; Mihailov, Stephen J.

This publication could be one of several versions: author's original, accepted manuscript or the publisher's version. / La version de cette publication peut être l'une des suivantes : la version prépublication de l'auteur, la version acceptée du manuscrit ou la version de l'éditeur.

For the publisher's version, please access the DOI link below. / Pour consulter la version de l'éditeur, utilisez le lien DOI ci-dessous.

Publisher's version / Version de l'éditeur:

<https://doi.org/10.1364/OE.476872>

Optics Express, 30, 26, p. 47361, 2022-12-19

NRC Publications Archive Record / Notice des Archives des publications du CNRC :

<https://nrc-publications.canada.ca/eng/view/object/?id=217518f4-7aba-43f7-88cf-5ee131e7a198>

<https://publications-cnrc.canada.ca/fra/voir/objet/?id=217518f4-7aba-43f7-88cf-5ee131e7a198>

Access and use of this website and the material on it are subject to the Terms and Conditions set forth at

<https://nrc-publications.canada.ca/eng/copyright>

READ THESE TERMS AND CONDITIONS CAREFULLY BEFORE USING THIS WEBSITE.

L'accès à ce site Web et l'utilisation de son contenu sont assujettis aux conditions présentées dans le site

<https://publications-cnrc.canada.ca/fra/droits>

LISEZ CES CONDITIONS ATTENTIVEMENT AVANT D'UTILISER CE SITE WEB.

Questions? Contact the NRC Publications Archive team at

PublicationsArchive-ArchivesPublications@nrc-cnrc.gc.ca. If you wish to email the authors directly, please see the first page of the publication for their contact information.

Vous avez des questions? Nous pouvons vous aider. Pour communiquer directement avec un auteur, consultez la première page de la revue dans laquelle son article a été publié afin de trouver ses coordonnées. Si vous n'arrivez pas à les repérer, communiquez avec nous à PublicationsArchive-ArchivesPublications@nrc-cnrc.gc.ca.



Nanoscale morphology and thermal properties of low insertion loss fiber Bragg gratings produced using the phase mask technique and a single femtosecond laser pulse

CYRIL HNATOVSKY,¹ KASTHURI DE SILVA,¹
NURMEMET ABDUKERIM,²  ROBERT B. WALKER,¹ HUIMIN DING,¹
AND STEPHEN J. MIHAILOV^{1,*} 

¹National Research Council Canada, 100 Sussex Drive, Ottawa, ON, K1A 0R6, Canada

²Infinera Corporation, 6373 San Ignacio Avenue, San Jose, CA 95119, USA

*stephen.mihailov@nrc-cnrc.gc.ca

Abstract: Fiber Bragg gratings with a very low insertion loss are inscribed using the phase mask technique and a single infrared (800 nm) femtosecond laser pulse. The morphology of the resultant light-induced structural changes in the Ge-doped silica fiber (SMF-28) is analyzed using scanning electron microscopy. The electron microscopy images reveal that each Bragg grating period incorporates an elongated micropore embedded in a region of homogeneous material modification. The Bragg wavelength drift and reflectivity of fiber Bragg gratings produced with single pulses having the same energy but different duration (80 fs and 350 fs) are monitored for 1000 hours in the course of isothermal annealing at 1000°C. The annealing data demonstrate that both the isothermal Bragg wavelength drift and the decrease in the reflectivity of the fiber Bragg gratings under test are statistically slower for the 350 fs inscription pulses.

© 2022 Optica Publishing Group under the terms of the [Optica Open Access Publishing Agreement](#)

1. Introduction

Fabrication of fiber Bragg gratings (FBGs) using infrared (IR) femtosecond (fs) laser pulses [1] has a significant advantage over the much older technology based on using continuous-wave ultraviolet laser beams and ultraviolet nanosecond laser pulses [2–4], because Bragg gratings can now be inscribed in almost any optical fiber without the need to photosensitize [5] the fiber core. Multiphoton absorption of fs pulses inside transparent media is easily achieved if the pulses are focused sufficiently. The material surrounding the focal volume remains unaffected by the fs light passing through it, which nominally allows one to microstructure fibers in a 3-D fashion [6] and also inscribe FBGs through different types of protective coating [7–10].

To perform strain and temperature measurements in extreme environments (e.g., combustion chambers [11], gas turbines [12,13], nuclear reactor cores [14,15]), there exists a broad class of fs laser-written FBGs whose remarkable resilience to the elements is determined by the very nature of material modification induced in the fiber core region (e.g., microvoids [16–18] and nanogratings [19–21]), in addition to the inherent robustness of the silica-based host fibers. These kinds of refractive index change have been broadly classified as Type-II index change [13].

Studies on the deployment of fiber-optic sensors beyond the lab environment have identified two main techniques of IR fs laser inscription of FBGs suitable for high-temperature operation between 900 °C and 1100 °C, namely, i) FBGs made using the phase mask technique (PM-technique) [1] and ii) FBGs made using the point-by-point technique (PbP-technique) [7,22–27]. Using the PM-approach, thermally unstable or stable gratings (Type-I or Type-II index change, respectively) can be induced in silica based glass fibers depending on the irradiation intensity of the fs beam [28]. Type-II FBGs written either using the PbP- or PM-approach can survive at

1000 °C for multiple hours and are thus considered to be “stable” at this temperature. It is known, however, that the Bragg wavelength and reflectivity of fs laser-written 1000 °C-resistant FBGs change over time at that temperature and, as a matter of fact, at much lower temperatures [29,30]. Unfortunately, reports on the long-term high-temperature performance of such FBGs remain scarce [29] despite the obvious fact that this information is critical in assessing their functionality and usefulness as high-temperature optical sensors.

The toughness of such FBGs often comes with the cost of high insertion loss (i.e., broadband loss measured in transmission on the long-wavelength side with respect to the Bragg resonance) associated with the dramatic structural transformations induced in the core by the high-intensity fs pulses. Modification at the core/cladding interface in and of itself does not necessarily contribute to insertion loss. In fact, extremely low loss devices were created when FBGs were written in the Type-I regime simultaneously in both the core and cladding [31]. The insertion loss is one of the key parameters that determine how many point sensors can be concatenated in a single fiber and, as a result, the overall capabilities of the sensing system. More specifically, depending on the laser-writing conditions, insertion losses between 2×10^{-5} dB and 10^{-3} dB per grating period are typical for: i) nanogratings-based FBGs [32] produced using the PM-technique, laser focus scanning across the fiber core and multiple IR fs laser pulses, ii) FBGs produced using the PM-technique, laser focus scanning across the fiber core and multiple IR fs laser pulses [33] and iii) FBGs produced using the PM-technique and multiple IR fs laser pulses deposited into one location in the fiber core without focus scanning [29].

In this respect, FBGs fabricated using IR fs laser pulses and the PbP-technique are not very different from their counterparts fabricated using the PM-technique especially using intensities above the threshold for Type-II index change [28], exhibiting insertion losses in the range from 10^{-4} dB to 2×10^{-3} dB per grating period [7,22–27]. Each period of FBGs inscribed using the PbP-technique has always been assumed to consist of a nanovoid/microvoid surrounded by a compressed region of increased refractive index [24–27], which can be justified by numerous studies in which such structures were produced with very tightly focused high-intensity fs laser pulses in different bulk materials (i.e., not in optical fibers) [16–18]. However, the recent scanning electron microscopy (SEM) analysis of an FBG inscribed using the PbP-technique and IR fs laser pulses has shown that the FBG period actually incorporates a string of microvoids (i.e., not a single microvoid) aligned along the pulse propagation direction [34]. This observation emphasizes the importance of using high-resolution diagnostics to characterize the FBG microstructure in each particular case, as, in principle, it is the main parameter that defines the totality of optical, mechanical and thermal properties of the FBG under consideration.

In our previous publication [35], we showed that 1000 °C-resistant Bragg gratings whose cladding modes exceed 30 dB in transmission and spectrally span more than 250 nm can be produced in a standard telecom Ge-doped silica optical fiber (i.e., Corning SMF-28) by employing the PM-technique and depositing five IR fs laser pulses into the fiber core. In this work we concentrate on the properties of FBGs inscribed using the PM-technique and only one IR fs pulse. In this case, the insertion loss of the resultant FBGs becomes astonishingly low, namely $\approx 10^{-6}$ dB per grating period, which is conservatively an order of magnitude lower than the smallest corresponding value reported for Type-II structures in the literature for both the PM-technique and PbP-technique. The scanning electron microscopy (SEM) images of the cleaved fiber samples reveal that in this case each Bragg grating period incorporates an elongated micropore embedded into a region of homogeneous material modification. The observed morphology of the FBGs under consideration correlates with their robustness, which we show by annealing the samples at 1000 °C for more than 1000 hours. In addition, we demonstrate using SEM how the modification morphology is affected by the polarization state and duration of the IR fs pulses when multiple pulses, as in Ref. [35], are used for FBG inscription.

2. Experiment and experimental results

2.1. Material modification produced using the phase mask technique

In the first series of experiments (“Series 1” further down in the text) we used the classical optical setup for the PM-technique (Fig. 1(a)) [1] and a Ti-sapphire regeneratively amplified laser system (“fs laser” further down in the text), operating at a central wavelength (λ) of 800 nm, to fabricate 1000 °C-resistant low-loss FBGs. The Fourier-transform-limited pulse duration of the fs laser was 80 fs. The output linearly polarized fs laser beam (LB) was expanded ≈ 3.5 times along the fiber axis and focused into the fiber (F) through a 0th-order-nulled holographic phase mask (M) with a period (Λ_M) of 1.07 μm using a plano-convex cylindrical lens (CL) corrected for spherical aberration. The effective numerical aperture (NA) of the cylindrical lens was estimated to be 0.25.

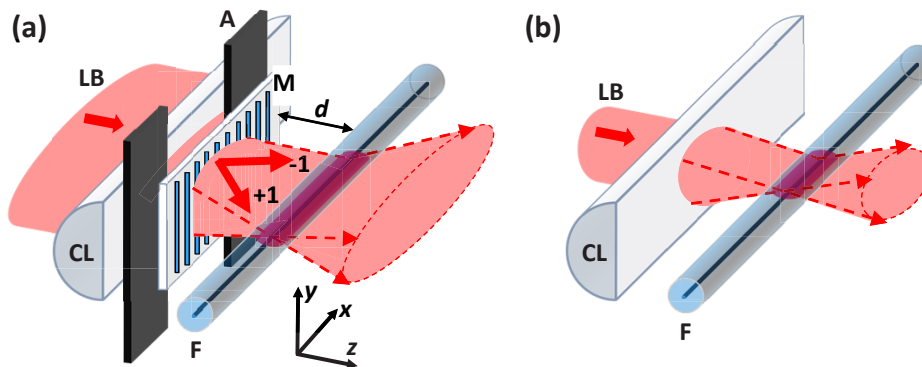


Fig. 1. Schematics of the two laser-writing configurations to photo-induce changes in the fiber core. (a) The setup to fabricate 1000 °C-resistant low-loss FBG using the PM-technique. The output laser beam (≈ 7 mm in diameter at the $1/e^2$ -intensity level) is expanded along the x -axis. (b) The setup in which the phase mask is removed from the optical path and the output laser beam is unexpanded. **LB** is the femtosecond laser beam; **M** is the holographic phase mask which generates only -1 and +1 diffraction orders at $\lambda = 800$ nm; **CL** is the focusing cylindrical lens; **A** is the 15 mm-wide aperture (along the x -axis) defined by the **CL**'s holder; **F** is the optical fiber; d denotes the mask-to-fiber distance (≈ 300 μm).

The beam expansion is required to produce a quasi-flat-top intensity distribution across the 15 mm clear aperture (**A**; Fig. 1) of the cylindrical lens. By keeping the peak light intensity in the line-shaped fs laser focus well above the intensity threshold to induce Type-II modification in the fiber core [28], a FBG consisting of a well-delineated region of Type-II modification along its full length can be produced. The Type-II modification is embedded into Type-I modification [28] which is formed where the intensity falls below the threshold for Type-II modification. At the very high annealing temperature used in the experiments, i.e., 1000 °C, the Type-I modification in the fiber material is completely erased [36] and a quasi-uniform Type-II FBG is thus created. This allows one to estimate the insertion loss per FBG period (η) by simply calculating the ratio of the FBG insertion loss and the number of periods in the FBG. Additionally, the FBG behavior during long-term annealing studies (see below) is easier to analyze if it is known that the light-induced modification pattern remains quasi-uniform along the FBG.

The front surface of the fiber (SMF-28; protective coating removed) was placed ≈ 300 μm away from the phase mask (i.e., $d \approx 300$ μm ; Fig. 1). At this d the photo-induced refractive index changes in the fiber core were strongest, which was determined by inscribing several Type-I FBGs at a fixed laser fluence but different d 's and measuring the reflectivity of the resultant FBGs. The optimum mask-to-fiber distance can be calculated based on the interplay of chromatic,

diffraction and aberration effects introduced by the laser-writing setup. The impacts of these effects, especially in the context of tight-focusing geometries and small-period phase masks, are rigorously analyzed in Ref. [37], where it is shown that there are two independent sets of phenomena that affect the size and shape of the focal volume after the phase mask. Specifically, these include: i) angular chromatic dispersion originating from the mask, counteracted by chromatic aberration of the cylindrical focusing lens and ii) spherical aberration caused by the mask substrate, counteracted by conical diffraction occurring at the mask. Approximate expressions to find the optimum d can be found in Ref. [38].

To inscribe FBGs, the fs laser was operated at 1 Hz and the pulses were fired at the fiber one at a time using a synchronized shutter. The morphology of the laser-induced modification in the fiber core was revealed using SEM on fiber samples cleaved approximately in the middle of the respective FBGs. No post-processing was performed on the fiber samples, i.e., the samples were not chemically etched and coated with a conducting material [21,39].

Figures 2(a) and 2(b) show SEM images of the fiber core irradiated in two separate locations along the fiber cross section with 80 fs pulses polarized along either the x -axis (i.e., along the fiber) or y -axis (i.e., perpendicularly to the fiber). The two spots were created by translating the laser focus $\approx 2 \mu\text{m}$ normal to the fiber axis. Two sets of samples were produced by depositing either 1 (Fig. 2(a)) or 5 (Fig. 2(b)) laser pulses per spot. The orientation of the linear laser polarization was adjusted by means of a half-wave plate. The FBGs, whose internal morphology is shown in SEM images in Fig. 2, were written at a peak light intensity that was ≈ 3 times higher than the threshold intensity for Type-II modification ($\approx 5 \times 10^{13} \text{ W/cm}^2$). The onset of Type-II structural changes in the fiber core in the single-pulse regime of irradiation, i.e., single-pulse threshold for Type-II modification, was determined using the dark-field microscopy technique described in Ref. [32]. The threshold intensity depended on the polarization of the fs pulses and was $\approx 15\%$ lower for y -polarized pulses than for x -polarized pulses, which can be explained using the formalism presented in Ref. [35].

The SEM images in Fig. 2(a) clearly show that for single-pulse irradiation every grating plane of the FBG is built of a highly elongated micropore ($\approx 0.15 \times 2 \mu\text{m}^2$) embedded into a region of homogeneous material modification with a much larger cross-sectional area ($\approx 0.7 \times 6 \mu\text{m}^2$). It is also noteworthy that there is no obvious dependence of the modification on the laser polarization in the single-pulse regime of irradiation. With 5 pulses deposited per spot, however, the micropores become noticeably expanded perpendicularly to the electric field E of the pulses (Fig. 2(b)).

In order to investigate how the pulse duration affects the modification morphology, the fiber core was irradiated with 3 Fourier-transform-limited 80 fs pulses (Fig. 3(a)) and 3 chirped 350 fs pulses (Fig. 3(b)). In both cases, the pulse polarization was perpendicular to the fiber axis and the laser fluence was the same. The pulses were chirped by adjusting the compressor of the fs laser and the pulse duration was measured with a single-shot autocorrelator.

Three conclusions can be deduced from Fig. 3. First, the elongated micropores produced with the 350 fs pulses stretch over the full length of the surrounding homogeneous modification, whereas the micropores produced with the 80 fs pulses are significantly shorter than the homogeneous modification region they are embedded into. Second, the peak intensity of the 350 fs pulses is roughly four times lower than that of the 80 fs pulses, however the homogeneous modification regions created with both the 80 and 350 fs pulses are qualitatively similar in terms of the size and shape, ($\approx 1 \mu\text{m}$ wide and $4 \mu\text{m}$'s long) and both possess elongated micropores inside them. Third, the modification morphologies produced with 1 (Fig. 2(a)), 3 (Fig. 3(a)) and 5 (Fig. 2(b)) 80 fs pulses look very much alike when the pulses are polarized perpendicular to the fiber. This is in contrast with the situation when the polarization of the pulses is parallel to the fiber, in which case the irradiation with 1 pulse (Fig. 2(a)) and 5 pulses (Fig. 2(b)) resulted in quite different modification morphologies.

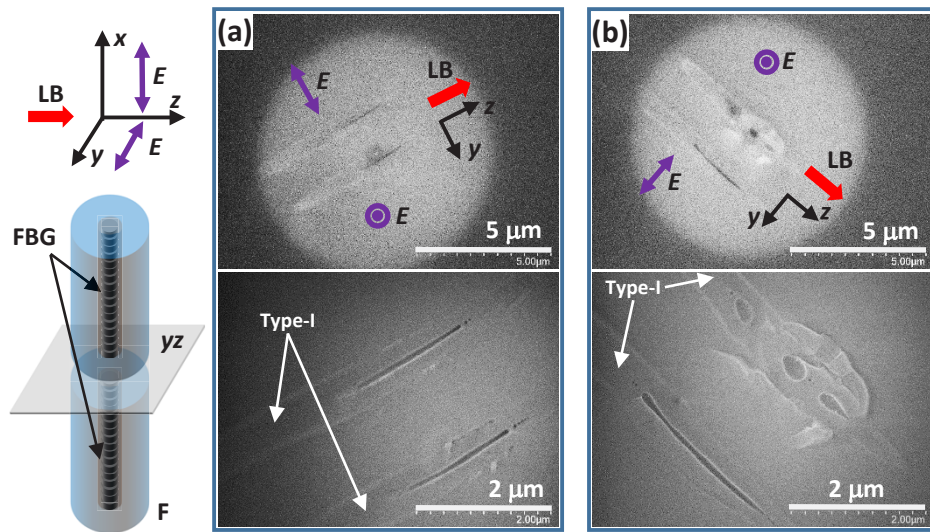


Fig. 2. SEM images of the material modification inside 1000 °C-resistant low-loss FBGs produced in SMF-28 by irradiating two separate spots, each with (a) one 80 fs pulse and (b) five 80 fs pulses. The top and bottom panels in (a) and (b) are SEM images in backscattered and secondary electrons, respectively. The orientation of the pulse polarization (E denotes the electric field of the pulses) is shown with purple double-sided arrows. “Type-I” denotes regions of homogeneous material modification. The samples were not chemically etched and coated with a conducting material.

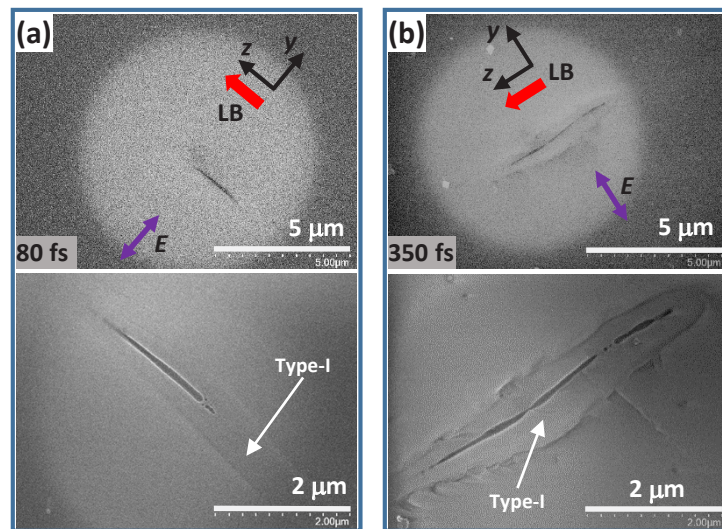


Fig. 3. SEM images of the material modification inside 1000 °C-resistant low-loss FBGs produced in SMF-28 with 3 (a) 80 fs pulses and (b) 350 fs pulses. The top and bottom panels in (a) and (b) are SEM images in backscattered and secondary electrons, respectively. The orientation of the pulse polarization (E denotes the electric field of the pulses) is shown with purple double-sided arrows. “Type-I” denotes regions of homogeneous material modification. The samples were not chemically etched and coated with a conducting material.

Measurements of the insertion loss of FBGs written with one fs pulse were performed using two different approaches, as presented in Fig. 4. In the first case, 10 separate FBGs were written along the fiber in the middle of the fiber core and the total insertion loss was measured (Fig. 4(a)). Each grating was 15 mm in length. In the other case, 10 FBGs were written one at a time across the fiber core by scanning the cylindrical lens along the y -axis and the total insertion loss was also measured (Fig. 4(b)). Even though modifications stacked across the fiber core and modifications placed in series along the fiber core interact differently with the probing electromagnetic field, the results obtained with these two complimentary approaches are useful for estimating the measurement error margins.

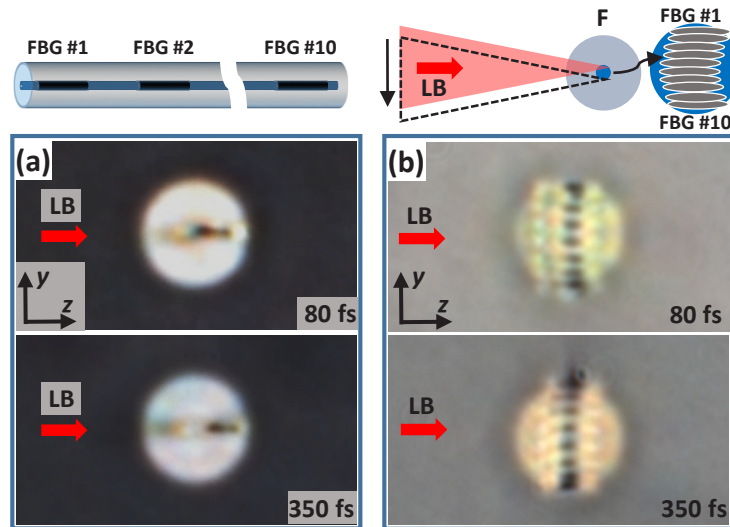


Fig. 4. Measuring the insertion loss of 1000 °C-resistant low-loss FBGs produced in SMF-28 with one pulse. (a) 10 separate FBGs are written along the core of SMF-28 and the total insertion loss is then measured. (b) 10 slightly overlapping FBGs are written across the core of SMF-28 and the total insertion loss is then measured. The top and bottom panels of (a) and (b) are optical microscopy images of the modification in the core of SMF-28 produced with one 80 fs pulse and one 350 fs pulse, respectively. The pulse polarization is parallel to the fiber axis, i.e., the x -axis. The core diameter of SMF-28 is $\approx 8 \mu\text{m}$.

As before, two different pulse durations were used in this experiment, namely Fourier-transform-limited 80 fs pulses and chirped 350 fs pulses. In both cases, the corresponding broadband insertion loss was measured ≈ 20 nm away from the Bragg resonance on the long-wavelength side, i.e., at 1570 nm. The total insertion loss for the FBG configurations presented in Fig. 4(a) and 4(b) varied depending on how accurately the modification was positioned with respect to the fiber axis. Also, regardless of whether 10 gratings were written either sequentially along the fiber length or stacked across the fiber core, a total insertion loss of 0.2 dB for both 80 fs and 350 fs pulses was never exceeded (i.e., ≈ 0.02 dB for each 15 mm-long FBG containing $\approx 2.8 \times 10^4$ periods). This means that the insertion loss per grating period was at the level of 10^{-6} dB (i.e., $\eta \approx 10^{-6}$ dB) based on a conservative estimate. No dependence of the insertion loss on the pulse polarization, i.e., whether the polarization was parallel or perpendicular to the fiber axis, was detected in the single-pulse inscription regime for both pulse durations. We note, however, that η showed a pronounced polarization dependence when 5 pulses were deposited into the same location in the fiber (Fig. 2(b)). The insertion loss in this regime for 80 fs pulses was on the average 0.04 dB per FBG (i.e., $\eta \approx 2 \times 10^{-6}$ dB) when the pulse polarization was perpendicular

to the fiber and 0.3 dB per FBG (i.e., $\eta \approx 1.5 \times 10^{-5}$ dB) when it was aligned along to the fiber. As in the previous cases, the gratings were 15 mm long containing $\approx 2.8 \times 10^4$ periods.

2.2. Material modification produced without the phase mask

In the second series of experiments (“Series 2” further down in the text), the phase mask was removed from the optical path and the unexpanded output fs beam of the fs laser was focused using the same cylindrical lens into SMF-28 to induce material modification in the core region. In Series 2, the pulse polarization was always perpendicular to the fiber and only Fourier-transform-limited 80 fs pulses were used for the laser writing. In order to be consistent with Series 1, the peak light intensity in Series 2 was also 3 times higher than the single-pulse intensity threshold for Type-II modification. The extent of Type-II modification along the core at this peak intensity was ≈ 5.3 mm. As before, the dark-field microscopy technique [32] was used to detect the emergence of Type-II structural changes in the fiber core.

The SEM images in Fig. 5 represent the situations when 1 (Figs. 5(a) and 5(d)), 2 (Fig. 5(b)) and 5 (Fig. 5(c)) fs pulses were deposited into the same location in the core. Similar to the observations from Series 1, the cross-sectional morphology of the light-induced structural changes in the fiber material mainly consists of micropores (microvoids) embedded into a region of homogeneous modification. While the micropores are clearly visible both in backscattered and secondary electrons, the extent of the homogeneous modification is better visualized by means of selective chemical etching in hydrofluoric acid (Fig. 5(d)) [39]. The micropores are now spherically shaped (≈ 0.2 μm in diameter for 1 pulse) and the homogeneous modification ($\approx 0.6 \times 11$ μm^2 for 1 pulse) extends well beyond the core boundary (central panel in Fig. 5(d)). Additionally, the homogeneous modification can now incorporate several (not just one) spherical nanopores aligned along the pulse propagation direction, which resembles the recently discovered morphology of FBGs inscribed using the PbP-technique [34]. In Fig. 5(c), one can also see a nascent nanocrack which lies between two spherical micropores. With more (e.g., tens) fs pulses deposited into the fiber, a system of planar nanocracks oriented perpendicular to the linear polarization of the pulses is expected to form [21].

To estimate the broadband insertion loss of the 5.3 mm-long laser-modified section of the fiber core, the fs beam was scanned perpendicular to the fiber (see Fig. 4(b)) to produce 10 single-pulse structures written one at a time across the fiber core. The total insertion loss was then measured at 1570 nm to be consistent with the measurements pertaining to Series 1. The insertion loss per structure was calculated to be ≈ 0.5 dB. If a 5.3 mm-long FBG with a 0.535 μm period (i.e., $\Lambda_M/2 = 0.535$ μm) had such an insertion loss, the respective effective loss per period (i.e., η_{eff}) would be equal to $\approx 5 \times 10^{-5}$ dB, which is at least 50 times higher than the typical values obtained for the FBGs from Series 1. When the peak intensity was reduced to twice the single-pulse intensity threshold for Type-II modification, the length of the corresponding modification decreased to ≈ 4.1 mm but the insertion loss per structure was still considerable, ≈ 0.2 dB. The η_{eff} (in the above sense) of such structures was $\approx 2.6 \times 10^{-5}$ dB, which is still much higher than the respective value obtained for the FBGs from Series 1. When the peak intensity was lowered even further, to exceed the threshold intensity by a factor of 1.5, the length of the structures decreased to ≈ 3.1 mm and, importantly, η_{eff} dropped drastically to $\approx 3.4 \times 10^{-6}$ dB. The latter result suggests that distinctive spherical nanopores, which mainly contribute to the insertion loss, cannot be formed at this intensity level. We also note that in Series 2 η_{eff} is seriously underestimated because, when the fs beam is not expanded and apertured as in Series 1, spherical nanopores are formed only in the central region of the structures where the intensity is high enough to produce microexplosions, whereas Type-II modification of unknown morphology at the ends of the structure has much lower insertion loss.

Table 1 compares the insertion losses of the above Type-II structures in the fiber core and the FBGs written with 80 fs pulses from Series 1.

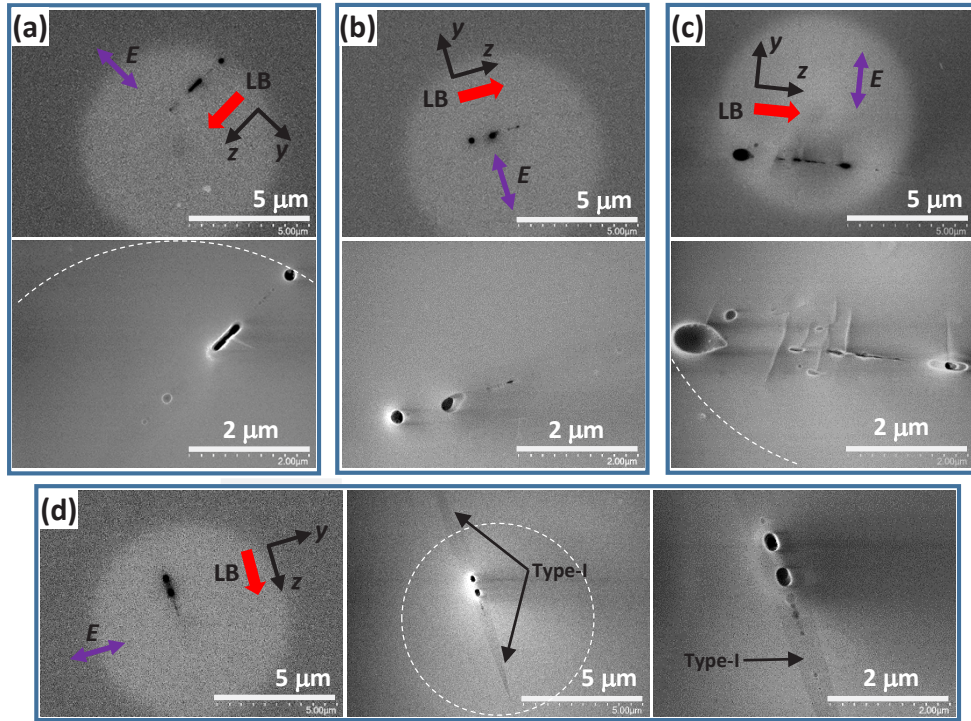


Fig. 5. SEM images of the material modification produced in the core of SMF-28 with the phase mask removed from the optical path (Fig. 1(b)). (a), (b) and (c) show the material modification produced with 1, 2 and 5 (five) 80 fs pulses, respectively. The top and bottom panels in (a), (b) and (c) are SEM images in backscattered and secondary electrons, respectively. The samples were not chemically etched and coated with a conducting material. (d) Chemically etched [39] uncoated samples produced with 1 (one) 80 fs pulse. The right panel and the two left panels are SEM images in backscattered and secondary electrons, respectively. The orientation of the pulse polarization (E denotes the electric field of the pulses) is shown with purple double-sided arrows. “Type-I” denotes regions of homogeneous material modification. Where it is possible, the white dashed lines are used to show the core-cladding boundary to better visualize the extent of material modification.

Table 1. Insertion losses of FBGs and structures inscribed without PM

Type of modification	Number of 80 fs laser pulses, N	Light intensity, (Type-II modification threshold) $\times k$	Polarization, parallel (x) or perpendicular (y) to fiber	Insertion loss, η or η_{eff}	
FBGs produced using PM-technique	FBG(1)	$N = 1$	$k \approx 3$	y	$\eta \approx 10^{-6}$ dB
	FBG(2)	$N = 1$	$k \approx 3$	x	$\eta \approx 10^{-6}$ dB
	FBG(3)	$N = 5$	$k \approx 3$	y	$\eta \approx 2 \times 10^{-6}$ dB
	FBG(4)	$N = 5$	$k \approx 3$	x	$\eta \approx 1.5 \times 10^{-5}$ dB
Structures produced without PM	Structure(1)	$N = 1$	$k \approx 3$	y	$\eta_{\text{eff}} \approx 5 \times 10^{-5}$ dB
	Structure(2)	$N = 1$	$k \approx 2$	y	$\eta_{\text{eff}} \approx 2.6 \times 10^{-5}$ dB
	Structure(3)	$N = 1$	$k \approx 1.5$	y	$\eta_{\text{eff}} \approx 3.4 \times 10^{-6}$ dB

2.3. Thermal stability of FBGs produced using the phase mask technique and a single fs pulse

To study the high-temperature performance of FBGs produced using one fs pulse, the prepared FBG samples were spliced to fiber pigtailed terminated with angled physical contact connectors and placed into a tube furnace for isothermal annealing at 1000 °C in ambient air. Two sets of FBG samples were prepared under the same laser-writing conditions except for the pulse duration: one set (3 FBGs) was prepared with Fourier-transform-limited 80 fs pulses and the other (3 FBGs) with chirped 350 fs pulses. The 6 FBG samples were accommodated in the same furnace. An external Type K thermocouple was placed in the furnace, in close proximity of the furnace's built-in thermocouple, and monitored using data acquisition software. The external thermocouple

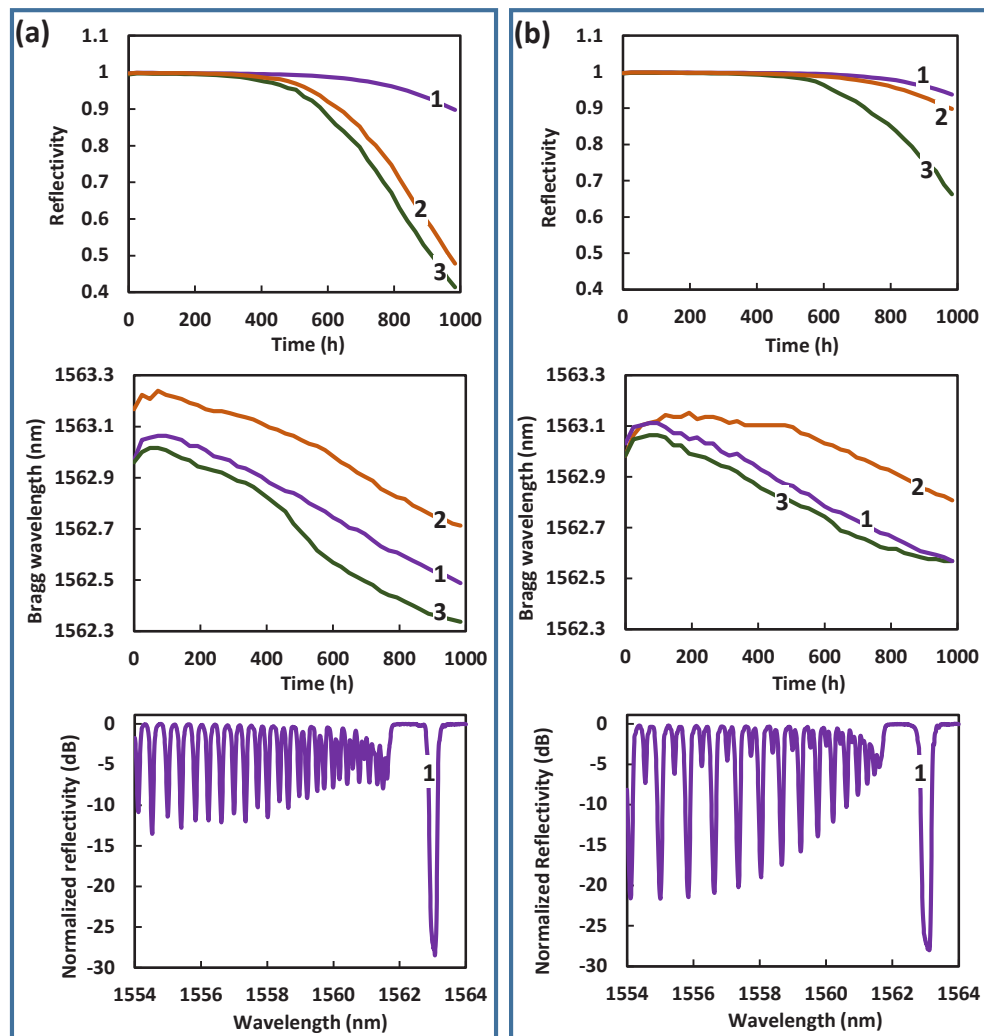


Fig. 6. Changes in the reflectivity and Bragg wavelength of FBGs inscribed in SMF-28 using the PM-technique and one fs pulse during isothermal annealing at 1000 °C. (a) Performance of 3 identical FBGs inscribed with one 80 fs laser pulse. (b) Performance of 3 identical FBGs inscribed with one 350 fs laser pulse. The bottom plots of (a) and (b) show the respective FBG transmission spectra recorded after 100 hours of annealing.

was necessary to provide redundancy in measuring the temperature inside the furnace in order to reduce the measurement error. The furnace was seen to fluctuate approximately $\pm 0.5^\circ\text{C}$ at 1000°C according to the thermocouple. This would correspond to a ± 7.4 pm fluctuation in the Bragg resonance [11]. The FBGs were centered within the furnaces, in-between the two thermocouples (external and internal), loosely resting in a hollow fused silica semi-cylinder so that they were free from stress and not touching the furnace side walls. Each FBG was monitored independently using a 16-channel FBG optical interrogator with an 8 pm wavelength resolution. Two separate interrogator channels were allocated per FBG: one channel to monitor the reflected light and the other for the light transmitted through the FBG and an optical isolator. Full spectrum optical data was collected every 5 hours, with the Bragg wavelengths being logged every half an hour in order to facilitate data processing and provide additional resolution in time.

The plots in Fig. 6 present long-term variations at 1000°C in the FBGs' reflectivities and Bragg wavelengths in transmitted light. The FBGs were produced using the same laser-writing conditions except for the pulse duration (i.e., 80 fs (Fig. 6(a)) versus 350 fs Fig. 6(b)). The top plots in Figs. 6(a) and 6(b) show that the FBGs' reflectivities remained essentially constant during the first 200 hours of isothermal annealing and only slowly decreased for the next 300 hours. During the last 500 hours of annealing the reflectivities of two FBGs produced with 80 fs pulses (green and orange traces) dropped to 40%-50%, while the reflectivities of all the FBGs produced with 350 fs were above the 60% level. The Bragg wavelengths of the FBGs (central plots in Figs. 6(a) and 6(b)), regardless of the pulse duration used for their inscription, showed more complex but quite consistent dynamics: a fast initial drift towards longer wavelengths, no drift, and a slow drift towards shorter wavelengths. When the FBGs were cooled down to room temperature, their Bragg wavelengths became on the average shorter by 520 pm in the case of 80 fs pulses and 400 pm in the case of 350 fs pulses compared with the respective values obtained on the original FBGs.

3. Discussions

3.1. Effects of focusing geometry on the material modification morphology

It was shown in Section 2 that laser inscription conducted using different focusing geometries (Series 1 and 2) can produce noticeably dissimilar modification morphologies in the fiber, which in turn leads to drastically different insertion losses for the resulting structures. The Type-II FBGs from Series 1 were classical devices inscribed by the PM-technique, whereas the structures from Series 2 were intended to imitate, albeit remotely, Type-II FBGs fabricated using the PbP-technique.

In Series 1 and 2, the light intensities (for the same pulse polarization and pulse duration) were scaled to be ≈ 3 times higher than the respective threshold intensities to induce Type-II modification (optical damage) in the fiber, but their actual magnitudes can only be estimated. For instance, in Ref. [35] we provided an approximate expression for light intensity in the fiber core (based on Series 1's geometry) in the absence of aberrations, neglecting focusing caused by the fiber itself, and ignoring self-focusing of the fs pulses in the fiber. The intensity required to produce the structures shown in Figs. 2 and 3(a) can then be estimated at 5×10^{13} W/cm² for 80 fs pulses. However, morphologically similar structures can be produced with 350 fs pulses (i.e., at a roughly 4 times lower intensity), implying that in Series 1 i) the intensity distribution rather than the intensity magnitude is responsible for the modification morphology and ii) self-focusing is not the dominant effect to define the intensity distribution inside the fiber.

For Series 1's geometry, aberrations caused by the oblique incidence (i.e., $\approx 50^\circ$) of focused fs pulses on the fiber surface are difficult to calculate. Some insight into the subject matter can be provided by ray theory models describing the refraction of a diagonally incident plane wave by a circular cylinder [40] which show that the shape of the interior caustics critically depends on the incidence angle. For Series 2's geometry, focused fs light impinges the fiber surface

approximately at a right angle (rather than at $\approx 50^\circ$ as in Series 1), which, in an ideal situation, would dramatically simplify the calculation of the intensity distribution inside the fiber. However, strong spherical aberration introduced by the mask substrate in the case of Series 2 (in Series 1 this aberration is compensated by conical diffraction when $d \approx 300 \mu\text{m}$) will significantly complicate the calculations. At this point we do not have an explanation of why the modification morphologies produced in Series 1 and 2 are so different.

3.2. *Bragg wavelength drift of FBGs produced using the phase mask technique and a single fs pulse*

While the possibility to fabricate 1000°C -resistant FBGs using the PM-technique and IR fs pulses was demonstrated more than a decade ago, there is still room to significantly improve or refine some important characteristics of these optical sensors. However, this work as well as previous reports clearly demonstrate that any Bragg grating inscribed in a silica-based fiber experiences a quite perceptible Bragg wavelength drift when subjected to 1000°C [29]. The magnitude and sign of the drift depend on the FBG and the host fiber, but the drift is essentially an unavoidable phenomenon that should be taken into account when high accuracy of long-term temperature monitoring using FBGs is required. This can be seen by converting the Bragg wavelength shift (i.e., the integral of Bragg wavelength drift over time) into a fictitious short-term temperature variation (i.e., an error in temperature measurements) that would cause a Bragg wavelength shift of the same magnitude. More specifically, to compete with standard high-temperature thermocouples in terms of accuracy, the wavelength shift of a FBG should not exceed a few tens of picometers if one assumes that a 14.8 pm change at 1000°C in the Bragg wavelength corresponds to a 1°C temperature variation [11]. So far, a measurement error that is comparable in the above context to that of high-quality thermocouples, i.e., $\approx 1^\circ\text{C}$ during hundreds of hours of exposure to 1000°C , cannot be achieved by any Type-II FBG, including the FBGs under discussion. We would also like to mention that rapid temperature variations in time are typical of many real-world operating conditions and in this respect it is important to know how repeated and rapid temperature cycling would affect FBG-based temperature sensors used for process monitoring, specifically i) their isothermal Bragg wavelength drift and ii) the reproducibility of their Bragg wavelength at a given high temperature.

There are several possible ways to mitigate the effects of the Bragg wavelength drift at high temperature. For instance, the FBGs can be pre-annealed at 1000°C - 1100°C to completely remove Type-I modification (and its effects on the Bragg wavelength drift) and then used at a lower temperature (e.g., 800°C) because the wavelength drift dramatically slows down with decreasing the surrounding temperature. Alternatively, the FBGs can be used for short (e.g., 1 hour) high-temperature measurements to keep the accumulated Bragg wavelength shift within acceptable margins. It is also probably possible to correct for the Bragg wavelength drift numerically. To do so, the FBGs must be fabricated under exactly the same conditions and also identically packaged in order to predict the temporal behavior of the Bragg wavelength drift using a calibration curve. Let us briefly discuss this option.

On the positive side, the results presented in Fig. 6 demonstrate that during the first 400 hours of annealing at 1000°C , variability within the two sets of identical FBGs with regards to the long-term changes in their reflectivities is not very large. With regards to their Bragg wavelengths, both sets of gratings display similar wavelength shifts of $\approx 0.7 \text{ pm/hour}$. We also note that variability in the drift rates among nominally identical FBGs over time is much more detrimental for temperature sensing applications than variability in the temporal behavior of their reflectivities. Indeed, the reflectivities of all the FBGs under test during the 1000-hours annealing experiment remained higher than 40%, which is totally sufficient to accurately measure their Bragg wavelengths. On the negative side, the observed 50 pm - 100 pm variability in wavelength shifts among identical FBGs at a specific time, (i.e., differences in Bragg wavelength at a given

time between green and orange traces in Fig. 6) immediately translates into a 3 °C-6 °C inaccuracy in temperature measurements between gratings.

We see two main causes of the variability in the Bragg wavelength shifts. First, it is the “packaging” issue. Although the acrylate coating was removed along the length of fiber in which the gratings were written, it is possible that unstripped regions of fiber can lead to changes in fiber stress. For instance, the burn-off of the acrylate fiber coating beyond the grating region can cause unequal amount of sticking of the samples to the fused silica semi-cylinder of the furnace, leading to different stresses in the FBG samples. The temperature at the ends of the silica semi-cylinder, which protruded several centimeters beyond the furnace’s walls, was much lower than the 1000 °C annealing temperature inside the furnace and the coating burn-off process in these locations was never fully completed. Because of the incomplete burn-off, some of the fiber samples could have also stuck to each other, as several samples were annealed in the furnace simultaneously. To this end, some of the samples were in contact with the external thermocouple’s sheath which became rough because of the oxidation caused by the prolonged exposure to atmospheric oxygen at 1000 °C. Finally, it is a well-known fact that high temperature exposure of fused silica optical fibers to moisture results in the degradation of their optical and mechanical properties [41,42]. Even though the relative humidity in our experiments was at the level of 40%, the multi-hour exposure of the FBG samples to water vapor made them brittle and hence definitely affected their spectral characteristics, possibly in a somewhat irregular fashion.

Second, it is a different degree of misalignment of the line-shaped laser focus and the fiber core among the FBG samples. As a consequence, the light-induced modifications associated with the FBGs had different angles with respect to the fiber axis and were differently offset with respect to the fiber axis. The superposition of the stress fields originating from the FBGs and the fiber core region was therefore different among the FBG samples under test. As a result, the stress relaxation dynamics occurring in the FBG samples at 1000 °C and the concomitant changes in the spectral characteristics of the FBGs was also different. We note that the misalignment issues can be easily alleviated by making the FBGs shorter.

4. Conclusions

We have shown that Type-II FBGs featuring a remarkably low insertion loss – comparable to that of Type-I FBGs of similar reflectivity – can be fabricated using the PM-technique and one IR fs pulse. High-resolution studies based on SEM demonstrate that each grating plane of the Type-II FBGs under consideration incorporates a single highly elongated micropore surrounded by a region of homogeneous modification. We speculate that low-loss Type-II FBGs based on such a modification morphology are easier to produce using the PM-technique than the PbP-technique. Annealing tests performed on the FBG samples demonstrate that the grating structure can survive 1000 °C for hundreds of hours. The annealing data also show that the isothermal Bragg wavelength drift of gratings inscribed with 80 fs and 350 fs pulses is similar, which implies that there exists a reasonably broad parameter space allowing the fabrication of low-loss Type-II FBGs. There is also evidence that the effect of the Bragg wavelength drift on the temperature measurements accuracy can be mitigated by using a calibration curve that would predict the FBG behavior at a constant high temperature over time. Taking into account that laser writing using the PM- technique is very robust and reproducible, the proposed recipe to fabricate 1000 °C-resistant low-loss Type-II FBGs is important for mass production of high-temperature optical sensors.

Disclosures. The authors declare no conflicts of interest related to this article.

Data availability. Data underlying the results presented in this paper are not publicly available at this time but may be obtained from the authors upon reasonable request.

References

1. S. J. Mihailov, C. W. Smelser, P. Lu, R. B. Walker, H. Ding, D. Grobnic, G. Henderson, and J. Unruh, "Fiber Bragg gratings made with a phase mask and 800-nm femtosecond radiation," *Opt. Lett.* **28**(12), 995–997 (2003).
2. K. O. Hill, Y. Fujii, D. C. Johnson, and B. S. Kawasaki, "Photosensitivity in optical fiber waveguides: application to reflection filter fabrication," *Appl. Phys. Lett.* **32**(10), 647–649 (1978).
3. G. Meltz, W. W. Morey, and W. H. Glenn, "Formation of Bragg gratings in optical fibers by a transverse holographic method," *Opt. Lett.* **14**(15), 823–825 (1989).
4. K. O. Hill, B. Malo, F. Bilodeau, D. C. Johnson, and J. Albert, "Bragg gratings fabricated in monomode photosensitive optical fiber by UV exposure through a phase mask," *Appl. Phys. Lett.* **62**(10), 1035–1037 (1993).
5. P. J. Lemaire, R. M. Atkins, V. Mizrahi, and W. A. Reed, "High pressure H₂ loading as a technique for achieving ultrahigh UV photosensitivity, and thermal sensitivity in GeO₂ doped optical fibres," *Electron. Lett.* **29**(13), 1191–1193 (1993).
6. R. R. Gattass and E. Mazur, "Femtosecond laser micromachining in transparent materials," *Nat. Photonics* **2**(4), 219–225 (2008).
7. A. Martinez, I. Y. Khrushchev, and I. Bennion, "Direct inscription of Bragg gratings in coated fibers by an infrared femtosecond laser," *Opt. Lett.* **31**(11), 1603–1605 (2006).
8. S. J. Mihailov, D. Grobnic, and C. W. Smelser, "Efficient grating writing through fibre coating with femtosecond IR radiation and phase mask," *Electron. Lett.* **43**(8), 442–443 (2007).
9. M. Bernier, F. Trépanier, J. Carrier, and R. Vallée, "High mechanical strength fiber Bragg gratings made with infrared femtosecond pulses and a phase mask," *Opt. Lett.* **39**(12), 3646–3649 (2014).
10. D. Grobnic, C. Hnatovsky, and S. J. Mihailov, "Thermally stable type II FBGs written through polyimide coatings of silica-based optical fiber," *IEEE Photonics Technol. Lett.* **29**(21), 1780–1783 (2017).
11. R. B. Walker, H. Ding, D. Coulas, S. J. Mihailov, M. A. Duchesne, R. W. Hughes, D. J. McCalden, R. Burchat, R. Yandon, S. Yun, N. Ramachandran, and M. Charbonneau, "Combustor deployments of femtosecond laser written fiber Bragg grating arrays for temperature measurements surpassing 1000°C," *Proc. SPIE* **10194**, 316–330 (2017).
12. R. B. Walker, S. Yun, M. De Silva, N. Charest, C. Hnatovsky, P. Lu, D. Robertson, S. J. Mihailov, and P. Vena, "High temperature measurement of a low emission, high pressure combustor using femtosecond laser written fiber Bragg gratings," *Proc. SPIE* **10654**, 7–92 (2018).
13. S. J. Mihailov, D. Grobnic, C. Hnatovsky, R. B. Walker, P. Lu, D. Coulas, and H. Ding, "Extreme environment sensing using femtosecond laser-inscribed fiber Bragg gratings," *Sensors* **17**(12), 2909 (2017).
14. G. Laffont, R. Cotillard, N. Roussel, R. Desmarchelier, and S. Rougeault, "Temperature resistant fiber Bragg gratings for on-line and structural health monitoring of the next-generation of nuclear reactors," *Sensors* **18**(6), 1791 (2018).
15. M. A. S. Zaghloul, M. Wang, S. Huang, C. Hnatovsky, D. Grobnic, S. Mihailov, M.-J. Li, D. Carpenter, L.-W. Hu, J. Daw, G. Laffont, S. Nehr, and K. P. Chen, "Radiation resistant fiber Bragg grating in random air-line fibers for sensing applications in nuclear reactor cores," *Opt. Express* **26**(9), 11775–11786 (2018).
16. E. N. Glezer and E. Mazur, "Ultrafast-laser driven micro-explosions in transparent materials," *Appl. Phys. Lett.* **71**(7), 882–884 (1997).
17. S. Juodkazis, K. Nishimura, S. Tanaka, H. Misawa, E. G. Gamaly, B. Luther-Davies, L. Hallo, P. Nicolai, and V. T. Tikhonchuk, "Laser-induced microexplosion confined in the bulk of a sapphire crystal: evidence of multimegabar pressures," *Phys. Rev. Lett.* **96**(16), 166101 (2006).
18. E. G. Gamaly, S. Juodkazis, K. Nishimura, H. Misawa, B. Luther-Davies, L. Hallo, P. Nicolai, and V. T. Tikhonchuk, "Laser-matter interaction in the bulk of a transparent solid: Confined microexplosion and void formation," *Phys. Rev. B* **73**(21), 214101 (2006).
19. Y. Shimotsuma, P. G. Kazansky, J. Qiu, and K. Hirao, "Self-organized nanogratings in glass irradiated by ultrashort light pulses," *Phys. Rev. Lett.* **91**(24), 247405 (2003).
20. V. R. Bhardwaj, E. Simova, P. P. Rajeev, C. Hnatovsky, R. S. Taylor, D. M. Rayner, and P. B. Corkum, "Optically produced arrays of planar nanostructures inside fused silica," *Phys. Rev. Lett.* **96**(5), 057404 (2006).
21. R. Taylor, C. Hnatovsky, and E. Simova, "Applications of femtosecond laser induced self-organized planar nanocracks inside fused silica glass," *Laser Photonics Rev.* **2**(1-2), 26–46 (2008).
22. A. Martinez, M. Dubov, I. Khrushchev, and I. Bennion, "Direct writing of fibre Bragg gratings by femtosecond laser," *Electron. Lett.* **40**(19), 1170–1172 (2004).
23. A. Martinez, I. Khrushchev, and I. Bennion, "Thermal properties of fibre Bragg gratings inscribed point-by-point by infrared femtosecond laser," *Electron. Lett.* **41**(4), 176–178 (2005).
24. A. Martinez, M. Dubov, I. Khrushchev, and I. Bennion, "Photoinduced modifications in fiber gratings inscribed directly by infrared femtosecond irradiation," *IEEE Photonics Technol. Lett.* **18**(21), 2266–2268 (2006).
25. M. L. Åslund, N. Nemanja, N. Grothoff, J. Canning, G. D. Marshall, S. D. Jackson, A. Fuerbach, and M. J. Withford, "Optical loss mechanisms in femtosecond laser-written point-by-point fibre Bragg gratings," *Opt. Express* **16**(18), 14248–14254 (2008).
26. J. U. Thomas, N. Jovanovic, R. G. Becker, G. D. Marshall, M. J. Withford, A. Tünnermann, S. Nolte, and M. J. Steel, "Cladding mode coupling in highly localized fiber Bragg gratings: modal properties and transmission spectra," *Opt. Express* **19**(1), 325–341 (2011).

27. R. J. Williams, N. Jovanovic, G. D. Marshall, G. N. Smith, M. J. Steel, and M. J. Withford, "Optimizing the net reflectivity of point-by-point fiber Bragg gratings: the role of scattering loss," *Opt. Express* **20**(12), 13451–13456 (2012).
28. C. W. Smelser, S. J. Mihailov, and D. Grobnc, "Formation of Type I-IR and Type II-IR gratings with an ultrafast IR laser and a phase mask," *Opt. Express* **13**(14), 5377–5386 (2005).
29. D. Grobnc, C. Hnatovsky, S. Dedyulin, R. B. Walker, H. Ding, and S. J. Mihailov, "Fiber Bragg grating wavelength drift in long-term high temperature annealing," *Sensors* **21**(4), 1454 (2021).
30. S. Dedyulin, E. Timakova, D. Grobnc, C. Hnatovsky, A. D. W. Todd, and S. J. Mihailov, "Accurate measurements of a wavelength drift in high-temperature silica-fiber Bragg gratings," *Metrology* **1**(1), 1–16 (2021).
31. D. Grobnc, C. W. Smelser, S. J. Mihailov, R. B. Walker, and P. Lu, "Fiber Bragg Gratings with Suppressed Cladding Modes Made in SMF-28 with a Femtosecond IR Laser and a Phase Mask," *IEEE Photonics Technol. Lett.* **16**(8), 1864–1866 (2004).
32. C. Hnatovsky, D. Grobnc, D. Coulas, M. Barnes, and S. J. Mihailov, "Self-organized nanostructure formation during femtosecond-laser inscription of fiber Bragg gratings," *Opt. Lett.* **42**(3), 399–402 (2017).
33. D. Grobnc, C. Hnatovsky, and S. J. Mihailov, "Low loss Type II regenerative Bragg gratings made with ultrafast radiation," *Opt. Express* **24**(25), 28704–28712 (2016).
34. S. Bhardwaj, T. T. Fernandez, S. Gross, M. J. Withford, and M. J. Steel, "Quantitative morphology of femtosecond laser-written point-by-point optical fiber Bragg gratings," *Opt. Lett.* **47**(3), 453–456 (2022).
35. N. Abdikerim, D. Grobnc, C. Hnatovsky, and S. J. Mihailov, "High-temperature stable fiber Bragg gratings with ultra-strong cladding modes written using the phase mask technique and an infrared femtosecond laser," *Opt. Lett.* **45**(2), 443–446 (2020).
36. M. Cavillon, M. Lancry, B. Poumellec, Y. Wang, J. Canning, K. Cook, T. Hawkins, P. Dragic, and J. Ballato, "Overview of high temperature fibre Bragg gratings and potential improvement using highly doped aluminosilicate glass optical fibres," *J. Phys. Photonics* **1**(4), 042001 (2019).
37. N. Abdikerim, D. Grobnc, R. Lausten, C. Hnatovsky, and S. J. Mihailov, "Complex diffraction and dispersion effects in femtosecond laser writing of fiber Bragg gratings using the phase mask technique," *Opt. Express* **27**(22), 32536–32555 (2019).
38. S. J. Mihailov, C. Hnatovsky, N. Abdikerim, R. B. Walker, P. Lu, Y. Xu, X. Bao, H. Ding, M. De Silva, D. Coulas, and D. Grobnc, "Ultrafast laser processing of optical fibers for sensing applications," *Sensors* **21**(4), 1447 (2021).
39. R. S. Taylor, C. Hnatovsky, E. Simova, D. M. Rayner, M. Mehandale, V. R. Bhardwaj, and P. B. Corkum, "Ultra-high resolution index of refraction profiles of femtosecond laser modified silica structures," *Opt. Express* **11**(7), 775–781 (2003).
40. C. L. Adler, J. A. Lock, B. R. Stone, and C. J. Garcia, "High-order interior caustics produced in scattering of a diagonally incident plane wave by a circular cylinder," *J. Opt. Soc. Am. A* **14**(6), 1305–1315 (1997).
41. P. J. Lezzi, E. E. Evke, E. M. Aaldenberg, and M. Tomozawa, "Surface crystallization and water diffusion of silica glass fibers: causes of mechanical strength degradation," *J. Am. Ceram. Soc.* **98**(8), 2411–2421 (2015).
42. H. Rose and T. J. Bruno, "The observation of OH in annealed optical fiber," *J. Non-Cryst. Solids* **231**(3), 280–285 (1998).